Biosensors and Bioelectronics 140 (2019) 111342

Contents lists available at ScienceDirect

Biosensors and Bioelectronics

journal homepage: www.elsevier.com/locate/bios

Development of a structure-switching aptamer-based nanosensor for salicylic acid detection

Changtian Chen[c,1], Silu Feng[d,1], Mian Zhou[f], Chonghui Ji[e], Long Que[d,**], Wei Wang[a,b,c,*]

[a] State Key Laboratory of Protein and Plant Gene Research, School of Life Sciences, Peking University, Beijing, China
[b] Peking University - Tsinghua University Joint Center for Life Sciences, Beijing, China
[c] Department of Plant Pathology and Microbiology, Iowa State University, Ames, IA, USA
[d] Department of Electrical and Computer Engineering, Iowa State University, Ames, IA, USA
[e] Department of Genetics, Development and Cell Biology, Iowa State University, Ames, IA, USA
[f] School of Life Sciences, Capital Normal University, Beijing, China

ARTICLE INFO

Keywords:
Aptamer-based biosensing
Structure-switching SELEX
Nanopore thin film sensor
Salicylic acid detection
Plant extract

ABSTRACT

Salicylic acid (SA) is a phytohormone regulating immune responses against pathogens. SA and its derivatives can be found in diverse food products, medicines, cosmetics and preservatives. While salicylates have potential disease-preventative activity, they can also cause health problems to people who are hypersensitive. The current SA detection methods are costly, labor-intensive and require bulky instruments. In this study, a structure-switching aptamer-based nanopore thin film sensor was developed for cost-effective, rapid, sensitive and simple detection of SA in both buffer and plant extracts. SA is a challenging target for aptamer selection using conventional systemic evolution of ligands by exponential enrichment (SELEX) due to its small size and scarcity of reactive groups for immobilization. By immobilizing the SELEX library instead of SA and screening the library using a structure-switching SELEX approach, a high affinity SA aptamer was identified. The nanopore thin film sensor platform can detect as low as 0.1 μM SA. This is much better than the sensitivity of antibody-based detection method. This nanosensor also exhibited good selectivity among SA and its common metabolites and can detect SA in *Arabidopsis* and rice using only about 1 μl plant extracts within less than 30 min. The integration of SA aptamer and nanopore thin film sensor provides a promising solution for low-cost, rapid, sensitive on-site detection of SA.

1. Introduction

The plant hormone salicylic acid (SA) regulates diverse physiological processes including thermogenesis, flowering, germination, pathogen resistance and circadian clock function (Cleland and Ajami, 1974; Raskin et al., 1987; Rhoads and Mcintosh, 1992; Shakirova et al., 2003; White, 1979; Zhou et al., 2015). As a major defense hormone, exogenous SA treatment enhances resistance to biotrophic pathogens (White, 1979) and mutants with elevated endogenous SA levels are usually more resistant to biotrophic pathogens (Bowling et al., 1994; Clarke et al., 1998; Zhang et al., 2003). Therefore, quantification of SA is a routine in plant immunity research.

Besides the effect on plant health, SA and its derivative, aspirin (acetylsalicylic acid) also have profound impact on human health. Aspirin can lower the risk of death from oesophagus, colorectal and lung cancer, protect against cardiovascular disease and may prevent pre-eclampsia (Kim et al., 2014; Oyola and Kirley, 2015; Rothwell et al., 2011; Voelker, 2014). However, aspirin can also cause urticaria, angioedema, rhinitis and asthma to people that are hypersensitive (Kowalski et al., 2013). Besides the medicinal sources, dietary intake of SA is also considerable since SA occurs naturally in various fruits, vegetables, beverages, herbs and spices (Szkop et al., 2017). Indeed, SA has been detected in serum and urine of people who does not take aspirin (Shaukat et al., 2011) and the urine SA level of vegetarians not taking aspirin is comparable to patients taking 75 mg aspirin (Lawrence et al., 2003). It is very likely that SA from dietary source may exert similar beneficial and adverse effects as aspirin on human. Therefore, the amount of SA from medicinal, dietary and cosmetic sources need to be frequently determined to ensure the health of people with different SA sensitivities. Hence, there is a rising need for a low-cost, fast,

* Corresponding author. State Key Laboratory of Protein and Plant Gene Research, School of Life Sciences, Peking University, Beijing, China.
** Corresponding author.
E-mail addresses: lque@iastate.edu (L. Que), oneway1985@pku.edu.cn (W. Wang).
[1] These authors contributed equally to this work.

https://doi.org/10.1016/j.bios.2019.111342
Received 17 February 2019; Received in revised form 17 May 2019; Accepted 20 May 2019
Available online 24 May 2019
0956-5663/

sensitive and simple method that allows routine and on-site detection of SA.

The critical need for SA quantification resulted in the development of various SA detection methods. SA is routinely quantified by chromatography-based methods like high-performance liquid chromatography (HPLC) (Venema et al., 1996). Mass spectrometry (MS) or tandem MS coupled chromatography-based methods were also developed to allow simultaneous quantification of multiple plant hormones including SA (Balcke et al., 2012; Du et al., 2012; Engelberth et al., 2003; Li et al., 2011; Pan et al., 2010; Segarra et al., 2006). However these methods are labor-intensive, consume considerable amount of solvent and require bulky instruments for chromatographic separation and UV or fluorescence detection. Capillary electrophoresis (CE) was tested as an alternative to HPLC-based methods because of its faster speed, simpler sample preparation and lower cost (Chang et al., 2017; Chen et al., 2014). However CE uses extremely high voltage (well over 10 kV) for electrophoresis which may raise safety concerns to operators. An *Acinetobacter* sp. ADPWH_*lux* strain containing a SA-inducible operon was developed as an SA biosensor (Huang et al. 2005, 2006). However, the use of this biosensor is time-consuming and labor-intensive. *In situ* detection of SA has been realized using reverse iontophoresis (Gonzalez-Sanchez et al., 2015) and TiO_2 nanoparticles (Tseng et al., 2014). However, the low sensitivity of these methods makes them unreliable for quantification. Using SA antibody, enzyme-linked immunosorbent assays (ELISAs) have been used to quantify SA (Wang et al. 2001, 2002). Due to the cross-reactivity of the antibody, these assays suffer from limited specificity and accuracy.

Aptamers have emerged as an attractive replacement for antibodies. Compared to antibodies which are expensive and notorious for their lack of reproducibility between lots, aptamers have several advantages such as low cost and high uniformity owing to their synthetic nature (Bradbury and Pluckthun, 2015). Aptamers tolerate a wide range of pH and salt concentrations and can be easily modified to allow compatibility with diverse detection platforms. Importantly, aptamers are more stable at elevated temperature and thermal denaturation is reversible, making it ideal for on-site or even field application.

In this study, we developed an aptamer-based label-free SA nanosensor using a structure-switching SELEX strategy. The identified SA aptamer was incorporated onto a nanostructured Fabry-Perot interference (nanoFPI) sensor developed by our team previously (Feng et al., 2018; Song et al., 2017). The interference fringes of the reflected white light from the nanoFPI sensor are used as transducing signals for SA quantification.

2. Materials and methods

2.1. Chemicals and materials

11-Mecaptoundecanoic acid ($HSC_{10}COOH$, 99%), 8-mercapto-1-Octanol (HSC_8OH, 98%), N-(3-Dimethylaminopropyl)-N′-ethylcarbodiimide hydrochloride (EDC), N-hydroxysuccinimide (NHS), ethanolamine (EA), salicylic acid and 4-hydroxybenzoic acid (4-HBA) were purchased from Sigma. Phosphoric acid (PPA), ethyl acetate, cyclopentane, methyl salicylate and streptavidin magnetic beads were purchased from Fisher. Benzoic acid was purchased from VWR. Salicylic acid 2-O-β-D-glucoside was purchased from Toronto Research Chemicals. Lambda enzyme was purchased from Lucigen. The initial SELEX library, probes, primers and SA aptamer candidates were purchased from IDT and Bio Basic.

2.2. Structure-switching SELEX

200 µl of magnetic beads were resuspended with capture probes (50 µM) dissolved in 200 µl binding buffer (50 mM Tris, 137 mM NaCl, 5 mM $MgCl_2$, pH 7.4) to immobilize the probes onto the beads. 100 µl of snap cooled DNA was incubated with beads for 30 min with gentle agitation using the thermomixer at 25 °C. The beads were then washed three times using binding buffer, resuspended in binding buffer containing 200 µl SA and agitated on the thermomixer for 30 min. The supernatant was amplified using PCR with 5′-phosphorylated reverse primer using the following program.

95°C	2 min	
95°C	30 s	n Cycles
55°C	30 s	
72°C	30 s	
72°C	5 min	

The optimal cycle number of the PCR was first determined through a small scale trial based on the criteria that the optimal PCR cycle produces the most abundant products with the correct size without unwanted by-products. Asymmetric PCR was then performed to further enrich the target sequences using the following program.

95°C	2 min	
95°C	30 s	M cycles
55°C	30 s	
72°C	1 min	
72°C	5 min	

Similarly, the optimal cycle number of the PCR was first determined through a small scale trial based on the criteria that the optimal PCR cycle produces the most abundant products with the correct size without unwanted by-products. The PCR products were treated with lambda enzyme and then cleaned and concentrated with ssDNA/RNA Clean and Concentrator (Zymo Research). The concentrated ssDNA was used for next round of SELEX. Starting from the fourth round, the negative selection was performed before positive selection using 200 µl 4-HBA. The enrichment of screening process was confirmed and the candidate aptamers were revealed by HiSeq. The sequences of the initial SELEX library, probes and primers used for SELEX and subsequent HiSeq library generation and sequencing are listed below.

Oligo name	Sequence
Library	CTTTCCCTACACGACGCTCTTCCGATCT-N_{40}-CTGTAGGCACCATCAATAGATCG
7-mer Probe	GGGAAAG-Biotin
8-mer Probe	AGGGAAAG-Biotin
9-mer Probe	TAGGGAAAG-Biotin
Amplification-F	CTTTCCCTACACGACGCTCTTC
Amplification-R	Phos-CGATCTATTGATGGTGCCTACAG
SP-F	AATGATACGGCGACCACCGAGATCTACACTCTTTCCCTACACGACGCTCTT
SP-R-6	CAAGCAGAAGACGGCATACGAGATCGTGATCGATCTATTGATGGTGCCTACAG
SP-R-13	CAAGCAGAAGACGGCATACGAGATGATCTGCGATCTATTGATGGTGCCTACAG
SP-R-15	CAAGCAGAAGACGGCATACGAGATTTGACTCGATCTATTGATGGTGCCTACAG

2.3. Fabrication of the nanopore thin film-based sensor

The sketch and operational principle of the nanoFPI sensor are shown in Fig. S1a. The nanoFPI sensor consists of a layer of Au-coated nanopore thin film embedded in its FPI cavity (Zhang et al., 2010). The reflected optical signals (interference fringes) from the nanoFPI sensor were used as the transducing signals. When the effective refractive index and the effective thickness of the nanopore thin film inside the FPI cavity change due to the coating of the aptamer and the SA, the reflected interference fringes shift. The sensor was fabricated using a process flow as illustrated in Fig. S1b (Yin et al., 2014). Briefly, 10 nm Cr was deposited on a rigorously cleaned coverslip glass substrate, followed by depositing 2–3 μm thick Al (99.999%) by E-beam evaporation. Then a two-step anodization process was carried out, resulting in a layer of anodic aluminium oxide (AAO) nanopore thin film on glass substrate. Thereafter, 150 nm Al was coated on the AAO nanopore thin film, followed by a photolithography and a wet etching process to fabricate AAO nanopore thin film patterns using Al as the mask layer. Then Al was etched away. Then AAO-glass chip was fabricated after depositing a layer of 10 nm Au on the surface of the AAO nanopore thin film with a layer of Cr (5 Å) as an adhesion layer. A polydimethylsiloxane (PDMS) microfluidic chip was fabricated separately using a soft lithography process, and then bonded with the AAO-glass chip after 2-min oxygen plasma treatment of AAO glass chip and PDMS microfluidic chip, followed by assembling input and output plastic tubes. A photo of the sensor chip, which consists of arrayed nanoFPI sensors is shown in Fig. S1c. The representative SEM image of the fabricated AAO nanopore thin film is shown in Fig. S1d.

2.4. Surface functionalization

The Au-coated sensor surface was functionalized with SA aptamers through 1-ethyl-3-(3-dimethylaminopropyl) carbodiimide (EDC)/N-hydroxysulfosuccinimide (NHS) chemistry as shown in Fig. S2. Specifically, the sensor surface was immersed in the 0.1 mM (1:9) $HSC_{10}COOH/HSC_8OH$ solution for 30 min and then washed with ethanol. After the surface was dried, the surface was immersed in a solution of NHS and EDC (NHS 0.2M, EDC 0.05M) for 30 min. The sensor surface was washed with PBS buffer and then immersed in the 5 μM aptamer solution overnight. This was followed by loading of 100 μl 1 M ethanolamine (EA) to block the non-occupied sites activated by the EDC/NHS. Finally, the sensor surface was rinsed with the SELEX binding buffer to flush off non-specifically adsorbed proteins. At this stage, the sensor is ready for the measurement. The sequences of the SA aptamer candidates used for functionalization were listed below.

Oligo name	Sequence
SAapta1	/5AmMC12/CTTTCCCTACACGACGCTCTTCCGATCTTTCCCGTTACCCTTATCTCATGCCTGCACTTGATCATGGTCTGTAGGCACCATCAATAGATCG
SAapta2	/5AmMC12/CTTTCCCTACACGACGCTCTTCCGATCTTTCCCGTTACCTTTATCTCATGCCTGCACTTGATCATGGTCTGTAGGCACCATCAATAGATCG
SAapta3	/5AmMC12/CTTTCCCTACACGACGCTCTTCCGATCTGGAGCGTTTTTAATCTTTCCCTCTTTTCCCAACTTGCCTCTGTAGGCACCATCAATAGATCG
SAapta4	/5AmMC12/CTTTCCCTACACGACGCTCTTCCGATCTCGTCGTTGACTTTCCCACTTACCACGGATTGATTGTATGACTGTAGGCACCATCAATAGATCG
SAapta5	/5AmMC12/CTTTCCCTACACGACGCTCTTCCGATCTTTCCCACTATTTTGAAATAGTCATTCCCCTAAGTGATGGTCTGTAGGCACCATCAATAGATCG

2.5. Detection procedure

After the surface of the sensors has been functionalized with SA aptamers, a series concentrations of SA in the SELEX binding buffer and plant extracts as well as a series concentrations of 4-HBA, MeSA, SAG and BA were applied to the sensors followed by 30-min incubation. Then the readings were taken after several sequential washes. All assay parameters including concentrations of the SA and incubation times were optimized to obtain high sensitivity and high signal to noise ratio. Experiments for negative controls were carried out to employ the full assay procedure but without SA, 4-HBA, MeSA, SAG or BA.

2.6. SA extraction from plants

Arabidopsis leaves or rice aerial parts were ground to a fine powder in liquid nitrogen using a mortar and pestle. 8 g fine powder was transferred to a 50-ml falcon tube, mixed with 28 ml 90% methanol, vortexed and sonicated for 16 min. The supernatant was collected after centrifugation at 20,800 g for 5 min 2 ml 0.2 M NaOH was added to the supernatant. The combined supernatant was then dried in speed-vac at room temperature (RT) overnight. The residue was resuspended in 20 ml of 5% trichloracetic acid and sonicated for another16 min. The sample was centrifuged at 20,800 g for 5 min and the supernatant was collected. This sample was extracted two times by adding 20 ml of ethyl acetate-cyclopentane (1:1), vortexed, sonicated for 16 min and centrifuged at 20,800 g for 1 min. The organic phase was combined and dried in speed-vac RT. The dried extract was dissolved in 16 ml of SELEX binding buffer. The supernatant was filtered using a syringe-facilitated filter with pore size 0.2 μm. This plant extract was supplemented with or without SA to the concentrations needed.

2.7. Data acquisition and statistical analysis

The average shift of the fringes for the measured transducing signals of the nanoFPI sensors was obtained by (i) first obtaining the shift of each fringe peak relative to that of the blank Au-coated AAO surface or the shift after the SA aptamer have been immobilized on the AAO surface, then (ii) averaging the shift of all the peaks. The transducing signal of the same sample was measured at least on five sensors to obtain the average value. Nonlinear regression was performed to derive dissociation constant using GraphPad.

2.8. Circular dichroism spectroscopy

Circular dichroism spectra of 1 μM SAapta1 in the SELEX binding buffer mixed with buffer control, 40 μM SA, 4-HBA, MeSA, SAG or BA were recorded on a Jasco J-710 spectropolarimeter with a Peltier-controlled cell holder designed for standard 1 cm × 1 cm quartz cuvettes. The temperature of the sample holder was set to 25 °C. The scan was taken from 225 nm to 350 nm at a scanning speed of 100 nm/min and 1 nm bandwidth.

2.9. HPLC analysis

Detection of SA in plant extracts by HPLC was performed according to Halder et al. (Dhiman et al., 2015).

2.10. GC-MS analysis

C19 was added to the dried samples as an internal standard. Samples and SA standards were resuspended in 90% methanol and dried in GC vial in speed-vac at room temperature overnight. Silylation of dried samples was performed with BSTFA +1% TCMS (Sigma) at 60 °C for 30 min, and then subjected to GC-MS on 7890C gas chromatograph in tandem with a 5975C MSD under standard conditions using EI ionization. Separation column was an HP5MSI (30 m long, 0.250 mm ID, 0.25 μm film thickness). The oven program was as

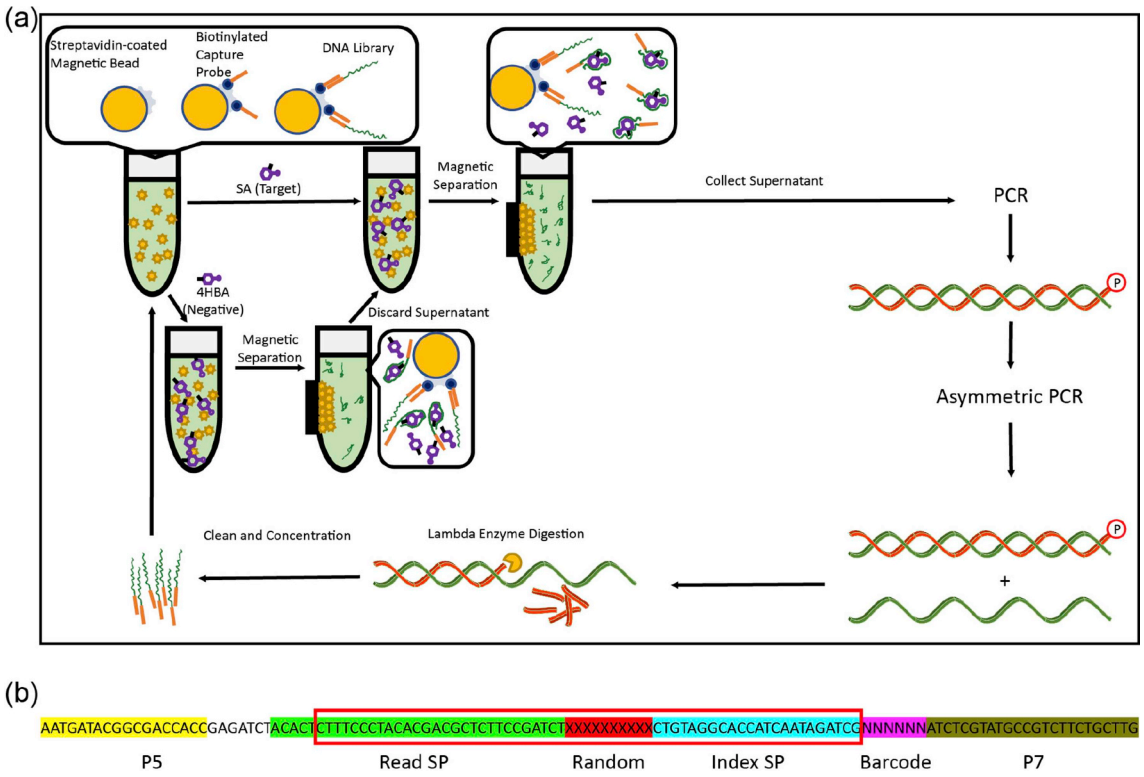

Fig. 1. (a) Pipeline of structure-switching SELEX; (b) Design of HiSeq-compatible SELEX library. The library sequence is highlighted by the red frame. P5 and P7 sequences are compatible with HiSeq. Read SP is the primer sequence for reading the 40 random nucleotides ("X" in the diagram). Index SP is the primer sequence for reading the 6-nucleotide index ("N" in the diagram). (For interpretation of the references to color in this figure legend, the reader is referred to the Web version of this article.)

follows: Initial temperature of 80 °C followed by, 5 °C/min ramp to 115 °C, then a ramp at 12.5 °C/min to 320 °C and a final hold for 7 min. The GC was controlled by the Agilent ChemStation software. Identification was performed by comparing the mass spectra to the NIST17 Library using Retention Indices.

3. Results and discussion

3.1. Structure-switching SELEX

Aptamers can be identified through an *in vitro* evolution technique called systematic evolution of ligands by exponential enrichment (SELEX). While the legacy SELEX method is able to identify aptamers for targets with high molecular weight with relative ease, small molecules like SA place great challenges to conventional SELEX. The small molecular size of SA makes size-based partition inefficient and the lack of chemical groups for immobilization makes wash-based separation challenging. To overcome these difficulties, we adopted a structure-switching SELEX strategy (Fig. 1a). The ssDNA library was hybridized to a short piece of capture complementary DNA (cDNA) immobilized on magnetic beads. Binding of SA induces conformational changes of binding sequences and subsequent de-hybridization from the capture cDNA. The nonbinders remain on the magnetic beads and can be removed. The SA binding sequences were further amplified through asymmetric PCR during which the complementary strand was phosphorylated at the 5′ end. The complementary strand was then removed using lambda exonuclease which is specific to the 5′-phosphorylated strand while the other strand was used as the library for the next SELEX round. After three rounds of positive selection against SA, negative selection with increasing concentrations of 4-hydroxybenzoic acid (4-HBA), a structure analog of SA was incorporated to enhance specificity. The length of the capture probe was increased to 8 and 9 during the round 14 and 15 respectively to increase the selection stringency.

The adapter sequences compatible with Illumina HiSeq platform have been included in the design of the SELEX library (Fig. 1b). The libraries from round 6, 13 and 15 were amplified, pooled and sequenced. The evolution of the relative frequency of the top five aptamer candidates was shown in Fig. 2a. The top candidate, SAapta1 has been

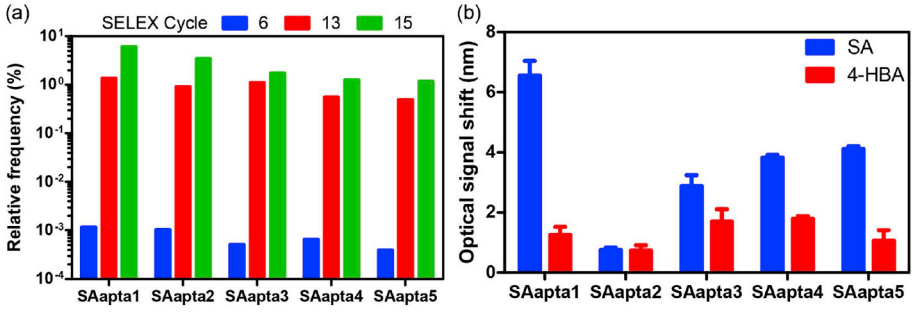

Fig. 2. (a) Relative frequency of the top five aptamer candidates over the 6th, 13th and 15th SELEX cycles; (b) Optical signal shift of the top five aptamer candidates using 40 μM SA or 4-HBA. Mean ± SEM was shown (n = 6).

enriched more than 5,000 fold comparing round 6 and 15, indicating the effectiveness of this structure-switching SELEX strategy. To identify the best aptamer candidate for further characterization, the top five candidates were functionalized onto the nanoFPI sensor and their binding affinity with SA and 4-HBA was screened (Figs. 2b, S1, S2). Among the five candidates, SAapta1 showed the highest affinity and good specificity. SAapta1 was thus selected for further characterization.

3.2. Determination of binding affinity of SAapta1 to SA

The dissociation constant (K_d) of SAapta1 was measured using a series of concentrations of SA (Fig. 3). Through nonlinear regression and statistical test of different binding models, we found that the "two sites specific binding" model fits the saturation curve best with the adjusted R^2 over 0.95. The K_d of the low affinity binding site is 4.703 μM while the K_d of the high affinity binding site is 34.57 nM, suggesting higher affinity than NPR4, the SA receptor in *Arabidopsis* (Fu et al., 2012).

The same concentration series of 4-HBA were also tested (Fig. 3). SAapta1 has limited affinity to 4-HBA. Importantly the optical fringe does not increase with the increasing concentrations of 4-HBA. Therefore, the observed optical fringe induced by 4-HBA simply represents a background signal. This demonstrates the effectiveness of the negative selection in the structure-switching SELEX.

3.3. Evaluation of binding kinetics of SAapta1

The binding kinetics of SAapta1 was investigated in order to determine the time for the binding reaction to achieve equilibrium (Fig. 4). When 40 μM SA was applied, it took about 30 min for the reaction to reach steady state while it took only 5 min when 0.2 μM SA was used. Therefore the steady state can be achieved faster when low concentration of SA is applied. This result is consistent with previous studies (Feng et al., 2018; Ferapontova et al., 2008). It takes more time for the higher concentration of SA to diffuse to the aptamers and reach the final equilibrium. Therefore methods like stirring which may accelerate diffusion can shorten the reaction duration (Zubtsov et al., 2006).

3.4. Assessment of binding sensitivity, specificity and inter-day variation of SAapta1

To test the binding sensitivity, we recorded the non-specific binding using the buffer alone. SA caused statistically significant more optical signal shift than the buffer even at the lowest concentration assayed

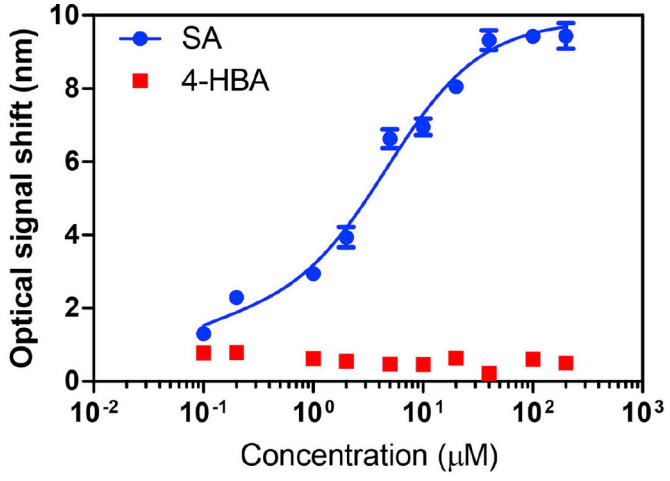

Fig. 3. Saturation curve of SAapta1 with SA and 4-HBA; Mean ± SEM was shown (n = 9).

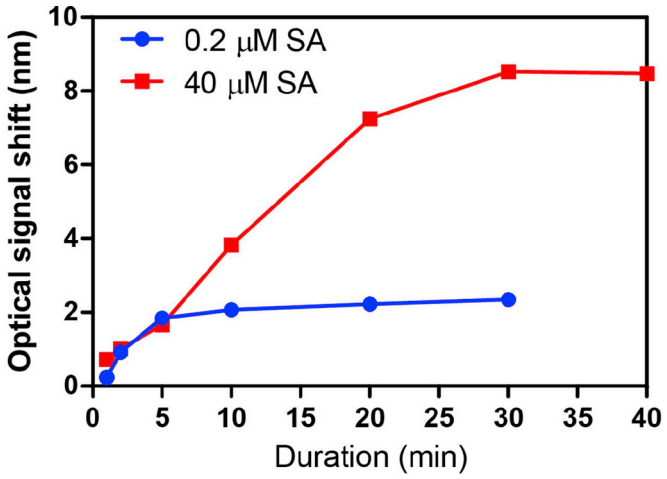

Fig. 4. Binding kinetics of SAapta1 with 0.2 μM and 40 μM SA. Mean ± SEM was shown (n = 6).

(0.1 μM) (Fig. 5a). Therefore the nanoFPI sensor is significantly more sensitive than the antibody-based method (Wang et al., 2002) and comparable to or even better than the bacteria-based biosensor (Huang et al. 2005, 2006). The detection limit of this aptamer-based nanosensor can be further and easily enhanced by varying the nanopore size as we have demonstrated previously for this type of nanoFPI sensor (Feng et al., 2018). However, it should be noted that the current detect limit is already sufficient for the detection of SA in plants (Defraia et al., 2008) as well as in the serum of human which is more than 1 μM (Shaukat et al., 2011). Therefore it is not critical to further improve the detection limit.

In plants, besides the free SA, most SA is glycosylated to form SA 2-*O*-*β*-glucoside (SAG) which serves as an inert reservoir of SA (Vlot et al., 2009). SA can also be methylated to form methyl salicylate (MeSA) which is also biologically inactive (Vlot et al., 2009). Since both of these SA metabolites still contain the SA moiety and they were not included in the negative selection in the structure-switching SELEX, we tested whether SAapta1 is able to distinguish them from SA (Fig. 5a). While 0.1 μM SAG only caused 0.31 nm optical fringe, 0.1 μM SA led to a much more pronounced optical fringe (1.30 nm). Even 100 μM SAG only resulted in 0.42 nm optical fringe while 100 μM SA generated 9.43 nm signal shift. In fact, SA induced significantly more optical signal shift than SAG at all the concentrations tested. The optical shift induced by SAG was not statistically different from that induced by buffer alone. It should be noted that the optical fringe did not increase with increasing concentrations of SAG. Therefore the signals generated by SAG are due to the non-specific binding with SAapta1. Similar results have been obtained for MeSA. However the optical fringe induced by MeSA is higher than SAG, though still much lower than SA. Since the methyl group of MeSA is much smaller than the glucose group of SAG and thus causes less steric hindrance, it is more likely for MeSA to partially occupy the binding pocket of SA on SAapta1 which explains its stronger non-specific binding. Besides SAG and MeSA, SA can also be converted to salicyloyl glucose ester (SGE), methyl salicylate *O*-*β*-glucoside (MeSAG) in plants (Fig. 5b). Since both SGE and MeSAG have chemical groups with more steric hindrance than the methyl group of MeSA, it is anticipated that SAapta1 may easily distinguish SGE and MeSAG from SA. Besides these SA conjugates which are larger than SA in molecular size, benzoic acid (BA) which is structurally similar to SA but smaller in molecular size, may bind SA aptamer without causing potential steric hindrance. Therefore, we also tested the binding affinity between BA and SAapta1 (Fig. 5a). The signals induced by BA were not statistically different from those induced by buffer at all concentrations surveyed. Therefore both the hydroxyl and the carboxyl groups are

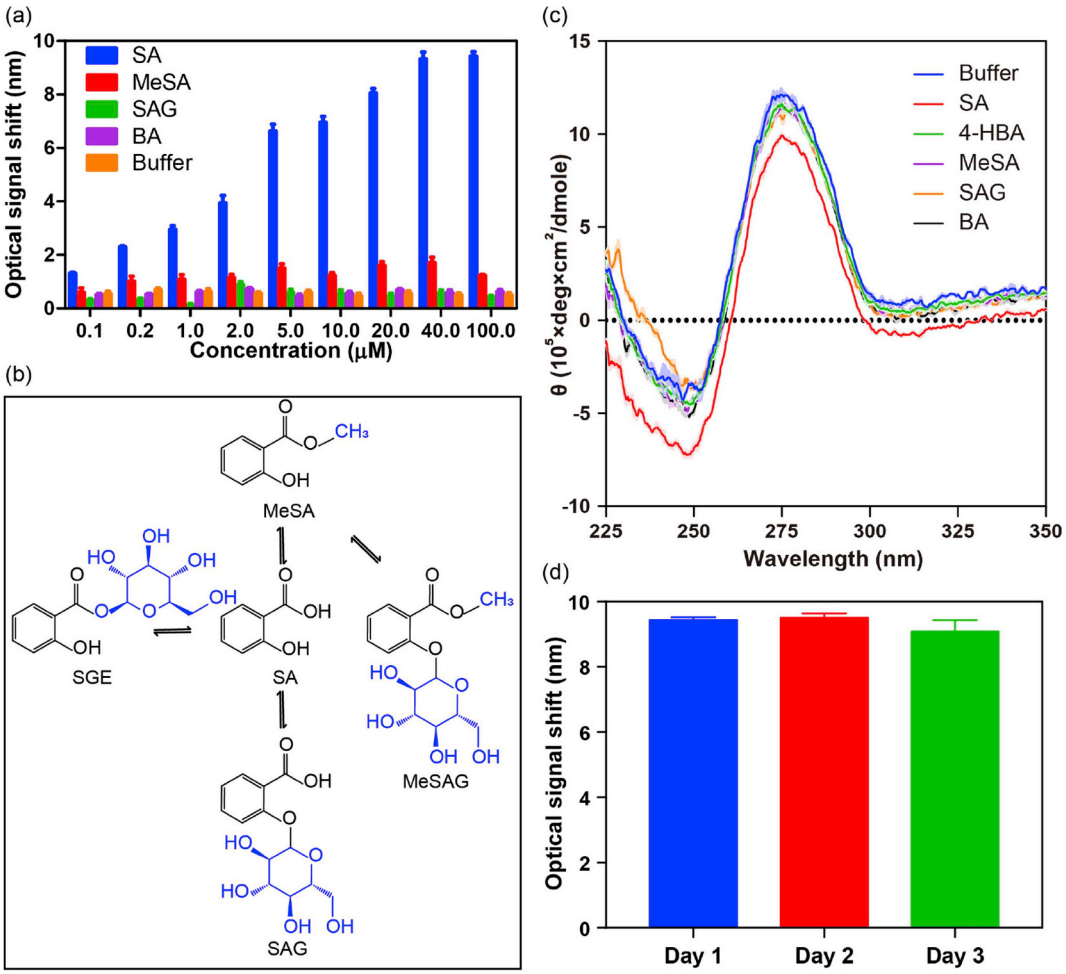

Fig. 5. (a) Optical signal shift induced by a series concentrations of SA, MeSA, SAG, BA and buffer only; Mean ± SEM was shown (n = 9). (b) SA metabolites and their structures.(c) The circular dichroism spectra of 1 μM SAapta1 in the SELEX binding buffer with buffer, 40 μM SA, 4-HBA, MeSA, SAG and BA. Mean ± SEM was shown (n = 3). SEM was shown as light colored area fill. (d) Optical signal shift of the same SA sample (40 μM) measured at three different days. Mean ± SEM was shown (n = 9). No statistical significant changes were detected using one-way ANOVA.

important to the binding specificity and affinity between SA and SAapta1.

To further verify the structural changes of SAapta1 induced by SA and confirm its binding specificity using a different detection method, we obtained the circular dichroism spectra of SAapta1 mixed with SA, 4-HBA, MeSA, SAG or BA (Fig. 5c). While SA caused dramatic structural changes, other SA metabolites and structural analogs showed negligible effects on the structure of SAapta1. Taken together, these results confirm SA-induced structure-switching of SAapta1 and suggest that SAapta1 has good specificity and can discriminate SA metabolites that were not included in the negative selection step.

We also tested the inter-day variation by measuring the sample SA sample on three different days (Fig. 5d). No statistical significant changes were detected by one-way ANOVA, suggesting that the measurement of the same sample recorded on different days do not differ from one another statistically. Therefore, we conclude that the nanoFPI sensor has good reproducibility in addition to its high sensitivity and specificity.

3.5. Detection of SA in plant extracts

To assess the feasibility of this aptamer-based nanoFPI sensor for SA detection in plant samples, the measurements of SA spiked in *Arabidopsis* extracts have been obtained (Fig. 6a). The optical signal shift increased with increasing concentrations of SA spiked in. The samples with plant extracts have significantly higher signal shifts than the samples without plant extracts at all the concentrations of spike-in SA. These results suggested that this type of sensor is able to detect the basal SA levels in *Arabidopsis*. Besides *Arabidopsis*, we further compared the performance of the nanoFPI sensor with HPLC using rice extracts (Fig. 6b). The nanoFPI sensor had statistically indistinguishable performance as HPLC. Binding specificity assay using pure MeSA solution showed that MeSA has low level non-specific binding to the sensor (Fig. 5a). To test whether the endogenous MeSA may interfere with the detection of SA in plant extracts, we performed GC-MS analysis (Fig. 6c). We found that our extraction method effectively excluded MeSA, making it barely detectable in the final extracts even by GC-MS. Therefore the non-specific binding of MeSA to the SAapta1 will not interfere with SA detection in plant extracts.

4. Conclusions

A structure-switching SELEX method was developed and an SA aptamer with high affinity and good specificity was successfully identified using this method. A nanopore thin film sensor based on this SA aptamer was developed for detection of SA in buffer and plant extracts from *Arabidopsis* and rice. This type of nanosensor enables detection of as low as 0.1 μM SA in buffer, which is significantly better than the sensitivity of antibody-based method. The kinetics of the binding between SAapta1 and SA has been studied. The signals can reach steady

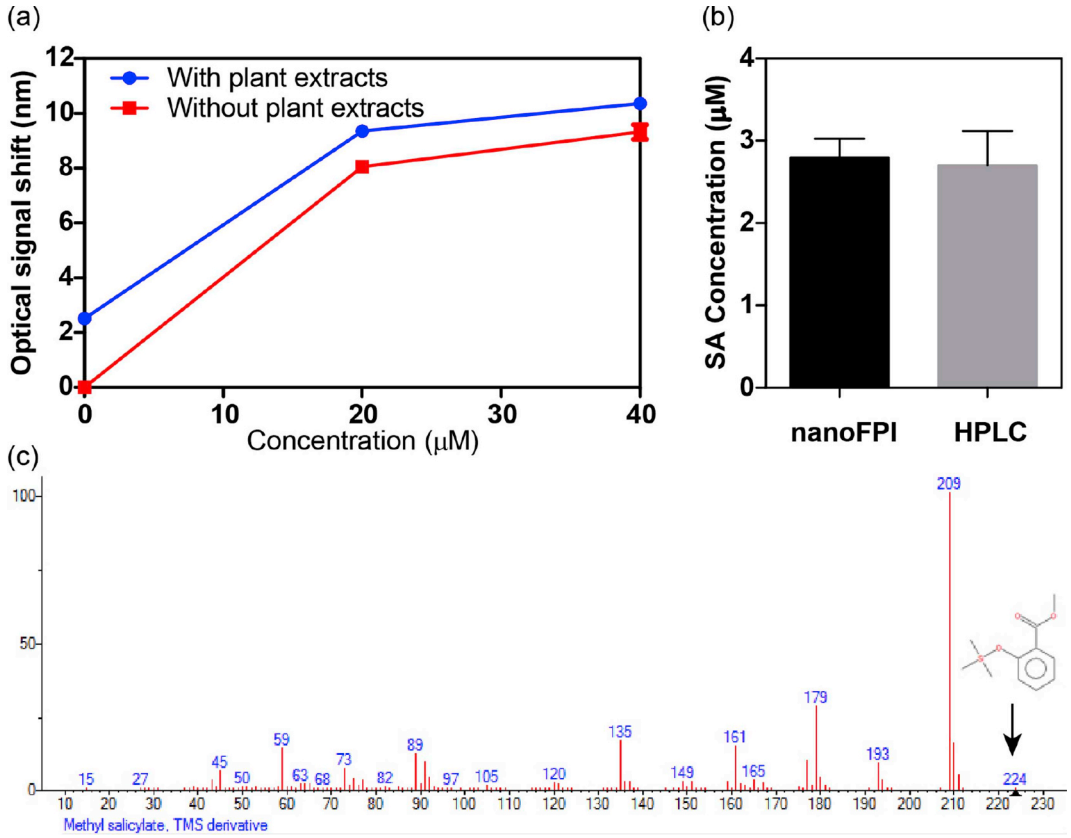

Fig. 6. (a) Optical signal shift of spike-in SA with and without *Arabidopsis* extracts. Mean ± SEM was shown (n = 9); (b) Comparison between nanoFPI and HPLC using rice extracts. No statistical significant changes were detected using Student's *t*-test. (c) Negligible detection of MeSA in rice extracts using GC-MS. The TMS derivative of MeSA corresponds to the 224 peak as indicated by the arrow which barely showed any signal.

state within 5 min when low concentration of SA is used. This type of sensor also has good specificity and can distinguish SA from its natural metabolites which also harbor SA moiety. The SA in plant extracts has also been detected successfully, suggesting the feasibility of this aptamer-based nanosensor. Therefore nanoFPI sensor provides a promising sensing platform for aptamer-based small molecule detection.

CRediT authorship contribution statement

Changtian Chen: Formal analysis. **Silu Feng:** Formal analysis. **Long Que:** Conceptualization, Writing - original draft, Writing - review & editing. **Wei Wang:** Conceptualization, Writing - original draft, Writing - review & editing.

Acknowledgements

We would like to thank Lucas Showman from the W. M. Keck Metabolomics Research Laboratory at Iowa State University for assistance with GC-MS and HPLC analysis. This research was funded in part by the startup funds from State Key Laboratory of Protein and Plant Gene Research, School of Life Sciences, Peking University and Peking University - Tsinghua University Joint Center for Life Sciences and USDA National Institute of Food and Agriculture, Hatch project 3808 to Wei Wang and NSF grant ECCS 1461841 to Long Que.

Appendix A. Supplementary data

Supplementary data to this article can be found online at https://doi.org/10.1016/j.bios.2019.111342.

References

Balcke, G.U., Handrick, V., Bergau, N., Fichtner, M., Henning, A., Stellmach, H., Tissier, A., Hause, B., Frolov, A., 2012. An UPLC-MS/MS method for highly sensitive high-throughput analysis of phytohormones in plant tissues. Plant Methods 8 (1), 47.

Bowling, S.A., Guo, A., Cao, H., Gordon, A.S., Klessig, D.F., Dong, X.I., 1994. A mutation in Arabidopsis that leads to constitutive expression of systemic acquired-resistance. Plant Cell 6 (12), 1845–1857.

Bradbury, A., Pluckthun, A., 2015. Standardize antibodies used in research: to save millions of dollars and dramatically improve reproducibility, protein-binding reagents must be defined by their sequences and produced as recombinant proteins, say Andrew Bradbury, Andreas Pluckthun and 110 co-signatories. Nature 518 (7537), 27–30.

Chang, Y.-H., Huang, C.-W., Fu, S.-F., Wu, M.-Y., Wu, T., Lin, Y.-W., 2017. Determination of salicylic acid using a magnetic iron oxide nanoparticle-based solid-phase extraction procedure followed by an online concentration technique through micellar electrokinetic capillary chromatography. J. Chromatogr. A 1479, 62–70.

Chen, W.-T., Wang, C.-I., Fu, S.-F., Lin, Y.-W., 2014. Analysis of salicylic acid in tobacco leaves using capillary zone electrophoresis with UV detection. GSTF J. Chem. Sci. 1 (2).

Clarke, J.D., Liu, Y.D., Klessig, D.F., Dong, X.N., 1998. Uncoupling PR gene expression from NPR1 and bacterial resistance: characterization of the dominant Arabidopsis cpr6-1 mutant. Plant Cell 10 (4), 557–569.

Cleland, C.F., Ajami, A., 1974. Identification of the flower-inducing factor isolated from aphid honeydew as being salicylic acid. Plant Physiol. 54 (6), 904–906.

Defraia, C.T., Schmelz, E.A., Mou, Z., 2008. A rapid biosensor-based method for quantification of free and glucose-conjugated salicylic acid. Plant Methods 4, 28.

Dhiman, H., Shubhasis, D., Easha, B., Pradipta, S., Umesh, C.H., Tapan, K.P., 2015. A rapid LC-ESI-MS/MS method for the quantitation of salicylic acid, an active metabolite of acetylsalicylic acid: application to in vivo pharmacokinetic and bioequivalence study in Indian healthy male volunteers. Appl. Clin. Res. Clin. Trial. Regulat. Affairs 2 (2), 90–102.

Du, F.Y., Ruan, G.H., Liu, H.W., 2012. Analytical methods for tracing plant hormones. Anal. Bioanal. Chem. 403 (1), 55–74.

Engelberth, J., Schmelz, E.A., Alborn, H.T., Cardoza, Y.J., Huang, J., Tumlinson, J.H., 2003. Simultaneous quantification of jasmonic acid and salicylic acid in plants by vapor-phase extraction and gas chromatography-chemical ionization-mass spectrometry. Anal. Biochem. 312 (2), 242–250.

Feng, S., Chen, C., Wang, W., Que, L., 2018. An aptamer nanopore-enabled microsensor for detection of theophylline. Biosens. Bioelectron. 105, 36–41.

Ferapontova, E.E., Olsen, E.M., Gothelf, K.V., 2008. An RNA aptamer-based electrochemical biosensor for detection of theophylline in serum. J. Am. Chem. Soc. 130 (13), 4256–4258.
Fu, Z.Q., Yan, S., Saleh, A., Wang, W., Ruble, J., Oka, N., Mohan, R., Spoel, S.H., Tada, Y., Zheng, N., Dong, X., 2012. NPR3 and NPR4 are receptors for the immune signal salicylic acid in plants. Nature 486 (7402), 228–232.
Gonzalez-Sanchez, M.I., Lee, P.T., Guy, R.H., Compton, R.G., 2015. In situ detection of salicylate in Ocimum basilicum plant leaves via reverse iontophoresis. Chem. Commun. 51 (92), 16534–16536.
Huang, W.E., Huang, L., Preston, G.M., Naylor, M., Carr, J.P., Li, Y., Singer, A.C., Whiteley, A.S., Wang, H., 2006. Quantitative in situ assay of salicylic acid in tobacco leaves using a genetically modified biosensor strain of Acinetobacter sp. ADP1 Plant J. 46 (6), 1073–1083.
Huang, W.E., Wang, H., Zheng, H., Huang, L., Singer, A.C., Thompson, I., Whiteley, A.S., 2005. Chromosomally located gene fusions constructed in Acinetobacter sp. ADP1 for the detection of salicylate. Environ. Microbiol. 7 (9), 1339–1348.
Kim, A.J., Lim, H.J., Ro, H., Ko, K.P., Han, S.Y., Chang, J.H., Lee, H.H., Chung, W., Jung, J.Y., 2014. Low-dose aspirin for prevention of cardiovascular disease in patients with chronic kidney disease. PLoS One 9 (8), e104179.
Kowalski, M.L., Asero, R., Bavbek, S., Blanca, M., Blanca-Lopez, N., Bochenek, G., Brockow, K., Campo, P., Celik, G., Cernadas, J., Cortellini, G., Gomes, E., Nizankowska-Mogilnicka, E., Romano, A., Szczeklik, A., Testi, S., Torres, M.J., Wohrl, S., Makowska, J., 2013. Classification and practical approach to the diagnosis and management of hypersensitivity to nonsteroidal anti-inflammatory drugs. Allergy 68 (10), 1219–1232.
Lawrence, J.R., Peter, R., Baxter, G.J., Robson, J., Graham, A.B., Paterson, J.R., 2003. Urinary excretion of salicyluric and salicylic acids by non-vegetarians, vegetarians, and patients taking low dose aspirin. J. Clin. Pathol. 56 (9), 651–653.
Li, Y.h., Wei, F., Dong, X.y., Peng, J.h., Liu, S.y., Chen, H., 2011. Simultaneous analysis of multiple endogenous plant hormones in leaf tissue of oilseed rape by solid-phase extraction coupled with high-performance liquid chromatography–electrospray ionisation tandem mass spectrometry. Phytochem. Anal. 22 (5), 442–449.
Oyola, S., Kirley, K., 2015. Another good reason to recommend low-dose aspirin. J. Fam. Pract. 64 (5), 301–303.
Pan, X., Welti, R., Wang, X., 2010. Quantitative analysis of major plant hormones in crude plant extracts by high-performance liquid chromatography–mass spectrometry. Nat. Protoc. 5 (6), 986.
Raskin, I., Ehmann, A., Melander, W.R., Meeuse, B.J., 1987. Salicylic Acid: a natural inducer of heat production in arum lilies. Science 237 (4822), 1601–1602.
Rhoads, D.M., Mcintosh, L., 1992. Salicylic-acid regulation of respiration in higher-plants - alternative oxidase expression. Plant Cell 4 (9), 1131–1139.
Rothwell, P.M., Fowkes, F.G.R., Belch, J.F.F., Ogawa, H., Warlow, C.P., Meade, T.W., 2011. Effect of daily aspirin on long-term risk of death due to cancer: analysis of individual patient data from randomised trials. Lancet 377 (9759), 31–41.
Segarra, G., Jauregui, O., Casanova, E., Trillas, I., 2006. Simultaneous quantitative LC-ESI-MS/MS analyses of salicylic acid and jasmonic acid in crude extracts of Cucumis sativus under biotic stress. Phytochemistry 67 (4), 395–401.
Shakirova, F.M., Sakhabutdinova, A.R., Bezrukova, M.V., Fatkhutdinova, R.A., Fatkhutdinova, D.R., 2003. Changes in the hormonal status of wheat seedlings induced by salicylic acid and salinity. Plant Sci. 164 (3), 317–322.
Shaukat, A., Grau, M.V., Church, T.R., Baxter, G., Barry, E.L., Summers, R., Sandler, R.S., Baron, J.A., 2011. Serum salicylate levels and risk of recurrent colorectal adenomas. Cancer Epidem. Biomar. 20 (4), 679–682.
Song, C., Chen, C., Che, X., Wang, W., Que, L., 2017. Detection of plant hormone abscisic acid (aba) using an optical aptamer-based sensor with a microfluidics capillary interface. In: Micro Electro Mechanical Systems (MEMS), 2017 IEEE 30th International Conference on. IEEE, pp. 370–373.
Szkop, M., Szkop, U., Kęszycka, P., Gajewska, D., 2017. A simple and robust protocol for fast RP-HPLC determination of salicylates in foods. Food Anal. Methods 10 (3), 618–625.
Tseng, P.-J., Wang, C.-Y., Huang, T.-Y., Chuang, Y.-Y., Fu, S.-F., Lin, Y.-W., 2014. A facile colorimetric assay for determination of salicylic acid in tobacco leaves using titanium dioxide nanoparticles. Anal. Methods 6 (6), 1759–1765.
Venema, D.P., Hollman, P.C.H., Janssen, K.P.L.T.M., Katan, M.B., 1996. Determination of acetylsalicylic acid and salicylic acid in foods, using HPLC with fluorescence detection. J. Agric. Food Chem. 44 (7), 1762–1767.
Vlot, A.C., Dempsey, D.A., Klessig, D.F., 2009. Salicylic Acid, a multifaceted hormone to combat disease. Annu. Rev. Phytopathol. 47, 177–206.
Voelker, R., 2014. USPSTF: low-dose aspirin may help reduce risk of preeclampsia. Jama 311 (20) 2055-2055.
Wang, S., Li, G., Xia, K., Xu, L., Chen, P., Zhou, X., 2001. Preparation and application of monoclonal antibodies specific for salicylic acid. Acta Bot. Sin. 43 (11), 1207–1210.
Wang, S., Xu, L., Li, G., Chen, P., Xia, K., Zhou, X., 2002. An ELISA for the determination of salicylic acid in plants using a monoclonal antibody. Plant Sci. 162 (4), 529–535.
White, R.F., 1979. Acetylsalicylic-acid (aspirin) induces resistance to tobacco mosaic-virus in tobacco. Virology 99 (2), 410–412.
Yin, H., Li, X., Que, L., 2014. Fabrication and characterization of aluminum oxide thin film micropatterns on the glass substrate. Microelectron. Eng. 128, 66–70.
Zhang, T., Gong, Z., Giorno, R., Que, L., 2010. A nanostructured Fabry-Perot interferometer. Optic Express 18 (19), 20282–20288.
Zhang, Y.L., Goritschnig, S., Dong, X.N., Li, X., 2003. A gain-of-function mutation in a plant disease resistance gene leads to constitutive activation of downstream signal transduction pathways in suppressor of npr1-1, constitutive 1. Plant Cell 15 (11), 2636–2646.
Zhou, M., Wang, W., Karapetyan, S., Mwimba, M., Marques, J., Buchler, N.E., Dong, X., 2015. Redox rhythm reinforces the circadian clock to gate immune response. Nature 523 (7561), 472–476.
Zubtsov, D.A., Ivanov, S.M., Rubina, A.Y., Dementieva, E.I., Chechetkin, V.R., Zasedatelev, A.S., 2006. Effect of mixing on reaction-diffusion kinetics for protein hydrogel-based microchips. J. Biotechnol. 122 (1), 16–27.